05,10

Growth of epitaxial thin films of Sr_2IrO_4 antiferromagnet for spintronics heterostructures

© I.E. Moskal[1], Yu.V. Kislinskii[1], A.M. Petrzhik[1], G.A. Ovsyannikov[1], N.V Dubitskiy[2]

[1] Kotelnikov Institute of Radio Engineering and Electronics, Russian Academy of Sciences, Moscow, Russia
[2] MIREA — Russian Technological University, Moscow, Russia

E-mail: ivan.moscal@yandex.ru

Received April 18, 2024
Revised April 18, 2024
Accepted May 8, 2024

A comparison of the parameters of epitaxial thin films of strontium iridate Sr_2IrO_4 obtained by two methods: cathode sputtering on direct current and cathode sputtering on pulsed current is presented. The resistive and crystallographic characteristics of the obtained thin-film samples are compared. The models of electronic transport of the obtained films are discussed: thermal activation, typical for a band dielectric, and three-dimensional hopping conductivity, characteristic of a Mott hopping conductor.

Keywords: antiferromagnetism, strontium iridate, epitaxial thin films.

DOI: 10.61011/PSS.2024.07.58977.58HH

1. Introduction

Recently, transition metal oxides have been of increased interest, primarily due to the presence of strong spin-orbit Interaction which causes the appearance of new types of materials: topological insulators [1], Weyl semimetals [2] and topological superconductors [3]. In strontium iridate Sr_2IrO_4, a high (with energy of the order of 0.5 eV) spin-orbital interaction is observed together with electron-electron interaction. Strontium iridate Sr_2IrO_4 is a representative of the 5d group and it is interesting for its electronic properties [4], as well as the crystal structure [5], similar to cuprate high-temperature superconductors. As a result, the contact resistance for the superconductor/Sr_2IrO_4 boundaries is small, which makes it possible to create Josephson junctiond based on spin-active materials used as elements of superconducting spintronics.

The parameters of thin films of strontium iridate strongly depend on the oxygen content, so $SrIrO_3$ demonstrates the properties of a paramagnetic metal, and an antiferromagnetic order occurs in Sr_2IrO_4 at temperatures below 240 K. There are a number of works in which films of the composition of iridates: $SrIrO_3$, Sr_2IrO_4 and Sr_3IrO_7 were obtained by laser ablation by the deposition from the same target, changing the oxygen content in the atmosphere of film growth [6,7].

It is known that a strontium iridate film, when deposited, may contain an admixture of iridium Ir and IrO_3 and may be multiphase, i. e. consisting of $SrIrO_3$, $SrIrO_3$and $Sr_3Ir_2O_7$ [7]. Multiphase significantly complicates the use of strontium iridate films in electronics.

Two-layer thin-film structures consisting of layers Sr_2IrO_4 and normal metal (N) attract great attention of researchers due to the possibility of their application in spintronics. Sr_2IrO_4/N heterostructures based on the Sr_2IrO_4 antiferromagnet are interesting for generating „pure“ spin current across the boundary, as well as submillimeter wave radiation

The paramagnetic $SrIrO_3$ and antiferromagnetic Sr_2IrO_4 may be of interest for superconducting electronics, in which superconducting heterostructures iridate/superconductor [8,9] are used to create Josephson junctions.

In this work, thin (nanometer-thick) Sr_2IrO_4 films were obtained by cathode sputtering at DC and pulsed currents. Their crystal and electric transport characteristics are discussed. A pulsed power supply allows to reduce the thermal load on the target and increase the power, leaving the thermal load at the same level. The switching power supply allows spraying dielectric and semiconductor targets without using an additional high-frequency generator.

2. Sputtering technique

For the synthesis of epitaxial films, a DC sputtering mode was used in the glow discharge mode in a diode configuration at a voltage between the target and the substrate of 400 V (DC mode). The second deposition option was carried out when setting the current by a switching power source (PC mode), which allowed to reduce the thermal load on the target and increase the deposition speed. A diode configuration was used with targets measuring targets diameter 25−30 mm, made of a material with a composition equal to the composition of the films being manufactured. The distance between the target and the sub-

strate with the heater was 50 mm. Typical growth rates were 3–4 nm/hours at DC mode and 10–15 nm/hours in pulsed sputtering mode. The substrate temperature during spraying was 820°C, and the operating pressure was 0.5 mbar.

The $SrIrO_3$ phase was synthesized from the Sr_2IrO_4 target using a mixture of gases from O_2 and Ar. Additional studies at different gas ratios, as well as the results obtained in [11], showed that the Sr_2IrO_4 film can be obtained by deposition in pure argon. At the same time, oxygen saturation of the film was carried out with subsequent oxygen content in the atmosphere at a temperature lower than by deposition temperature (500°C).

An $NdGaO_3$ (NGO) single crystal with an orientation in the plane (110) was used as a substrate, which makes it possible to consider it as a pseudocube with a lattice parameter $a_{NGO} = 0.386$ nm and an aspect difference of 0.12%, which in some cases gives induced magnetic anisotropy [10].

The targets were made from a mixture of $SrCO_3$ and IrO_2 powders, the powder with the ratio $Sr_{1.85}IrO_4$ was pressed into tablets, then heated to 900–1000°C for two days. The resulting powder was crushed and mixed with paraffin dissolved in hexane. After drying, the mixture was pressed into tablets with a diameter of 25 mm, corresponding to the diameter of the cathode from which by deposition was carried out. The tablets were baked at 1200°C for 20 h. [11]. X-ray phase analysis showed that the obtained targets are single-phase and have a tetragonal crystal lattice: $I4/mmm$ spatial group, lattice parameters: $a = 0.388$ nm, $c = 1.289$ nm. The obtained parameters are close to the tabular values for single crystals Sr_2IrO_4, which are 0.3888 and 1.290 nm [12], respectively.

3. Structural analysis of thin film Sr_2IrO_4

X-ray diffraction analysis of the parameters of the unit cell of the Sr_2IrO_4 film was carried out on a Rigaku smartLAB diffractometer equipped with a rotary copper anode. Diffraction measurements were carried out in the geometry of a parallel beam using a Ge(220)x2 monochromator for $K_{\alpha 1}$ diation with a wavelength of $\lambda = 0.1540$ nm. Scanning was performed in the $2\theta/\omega$ scanning mode to determine the phase composition of the film and its crystallographic orientation relative to the substrate. X-ray diffraction analysis of two thin films Sr_2IrO_4 grown on an $NdGaO_3$ substrate (Figure 1) revealed the presence of diffraction peaks corresponding to the materials of the film itself and the substrate. The absence of additional peaks characteristic of other crystalline phases of strontium and iridium oxides indicates the single-phase composition of the Sr_2IrO_4 film.

The films presented in the work have an c parameter equal to 1.280 nm for a film obtained in DC mode and 1.278 nm for a film obtained in PC mode (see Figure 2). In experimental works [7,12], it is reported that Sr_2IrO_4

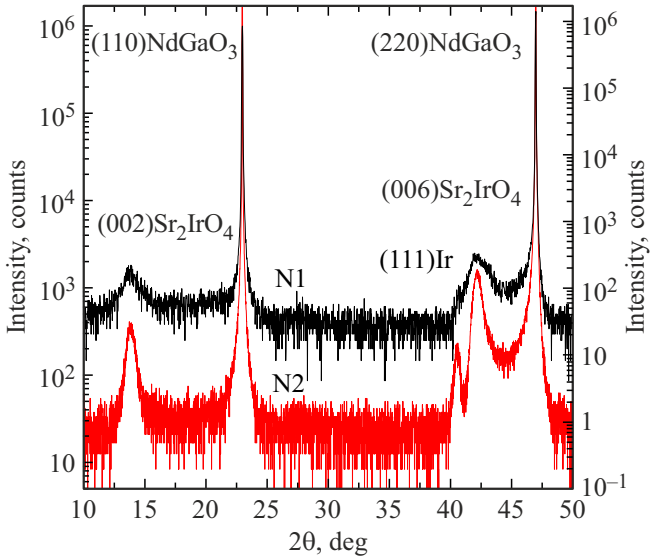

Figure 1. $2\theta/\omega$ X-ray diffractograms for 30 nm thick film N2 obtained in DC mode and for N1 film obtained in PC mode.

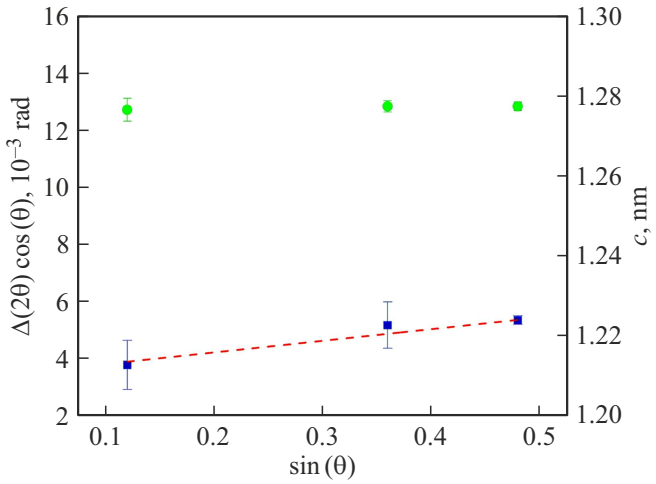

Figure 2. Dependence of $\Delta(2\theta)\cos\theta$ on $\sin\theta$ peaks (00n)Sr_2IrO_4 films N2. The dashed line indicates the straight line obtained from (1). Filled circles mark the values of the film lattice parameters c obtained for each of the peaks of the film.

films with c lattice parameters from 1.27 to 1.29 nm were obtained. Note that for a single crystal Sr_2IrO_4 c, the parameter has a value of 1.2887 nm.

The unitcell volume of the studied films, based on the measured values of the c parameter, is always less than that of the single crystal Sr_2IrO_4, which indicates a small nonstoichiometry in cations [13].

To quantify the degree of deformation of the crystal lattice in the studied Sr_2IrO_4 films, an analysis of the width of diffraction peaks on X-ray scans was performed (see Figure 2). According to the Scherrer formula [14], the half-widths of $\Delta(2\theta)$ peaks recorded on (00n) $2\theta/\omega$ scans are related to the relative deformation of the $\delta c/c$ lattice and

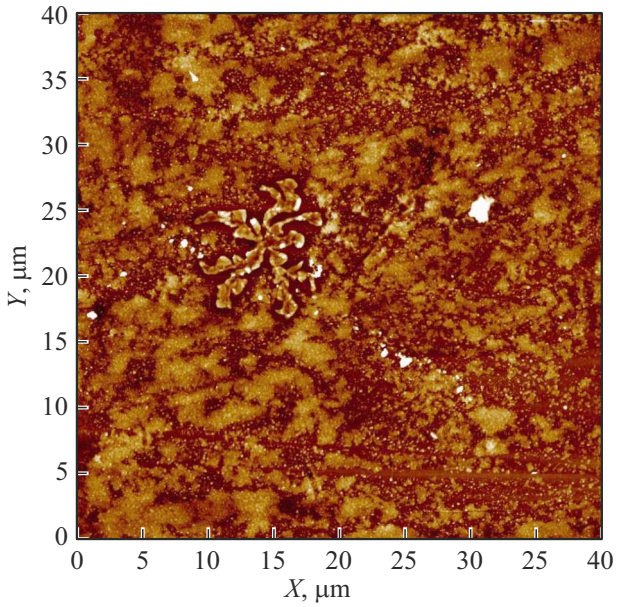

Figure 3. Scan of the surface of the Sr_2IrO_4 film with an admixture of polycrystalline iridium, a drop of which is visible in the center of the scanned area

the thickness of the coherent scattering t by the following ratio (1):

$$\Delta(2\theta) = \frac{0.9\lambda}{t \cdot \cos\theta} + \left(\frac{2\delta c}{c}\right) \cdot \tan\theta, \qquad (1)$$

where Δ — half-width of the diffraction peak of the scan $2\Theta/\omega$; t — film thickness or average size of crystalline grains; θ — diffraction angle; $\delta c/c$ — relative deformation of the interplane distance along the normal to the surface of the film; 0.1540 nm — X-ray wavelength $CuK_{\alpha 1}$.

Figure 2 shows the information received that $\Delta(2\theta) \cdot \cos\theta$ is from $\sin\theta$ for Sr_2IrO_4 N2 film. The dashed line indicates a straight line obtained from the ratio (1). The analysis of the approximation coefficients made it possible to calculate the thickness of the coherent scattering for the studied film $t \approx 30$ nm and to estimate the relative deformation from the $\delta c/c = 2 \cdot 10^{-3}$ crystal lattice parameter. The obtained value of $\delta c/c$ characterizes elastic deformations of the crystal structure of the film in the c direction.

Figure 1 shows peaks of iridium (111)Ir, which show that polycrystalline iridium is formed on the substrate along with the nucleation of the Sr_2IrO_4 film. The data obtained in an atomic force microscope (Figure 3) shows the appearance of iridium droplets on the surface of the film. The RMS roughness of the film in this case is a value comparable to the thickness of the film (RMS = 24 nm), which indicates the three-dimensional nature of the growth of films

4. Electro-transport characteristics

The study of the temperature dependence of the resistance $R(T)$ is necessary to understand the features of electronic transport in the obtained Sr_2IrO_4 films. The electrical resistance of the film was measured in the temperature range 80−300 K by the four-probe Montgomery method [15]. Platinum contacts were deposited by DC magnetron sputtering at room temperature.

Figure 4, *a* shows the obtained dependencies $R(T)$ for two films. It can be seen that the dependencies of $R(T)$ differ for the two films N1 and N2. For N1 at $T = 300$ K, the resistance value was 106 kΩ, and for the film N2 at $T = 300$ K, the resistance was significantly less than 4.5 kΩ. With a decrease in temperature, an increase in resistance is observed in both films. This behavior is typical for dielectric films. The resistance values at $T = 300$ K are probably different due to the presence of iridium inclusions in the film.

Exponential temperature dependence of resistance (2) for for both films indicates on the conductivity by thermal activation of carriers typical for systems with a gap in the excitation spectrum . In the thermal activation model, the resistivity of ρ depends on temperature

$$\rho(T) = \rho_0 \exp\left(\frac{\Delta E}{2kT}\right), \qquad (2)$$

where ΔE is the activation energy, k is the Boltzmann constant. The activation energy of ΔE is determined by the linear section of the $\rho(T)$ dependence in $\ln\rho$ coordinates depending on the reverse temperature of $1/T$, as shown in the inserts to Figure 4. The activation conductivity model approximates the $\rho(T)$ dependences well at liquid nitrogen temperatures. For sample N1, the activation energy value was $\Delta E \approx 65$ MeV, and for sample N2, the energy was $\Delta E \approx 22$ MeV. In works [10,12], the activation energies for thin films Sr_2IrO_4 ranged from 60 to 200 MeV, depending on the thickness of the film and the conditions of its deposition. We believe that a change in the plasma structure

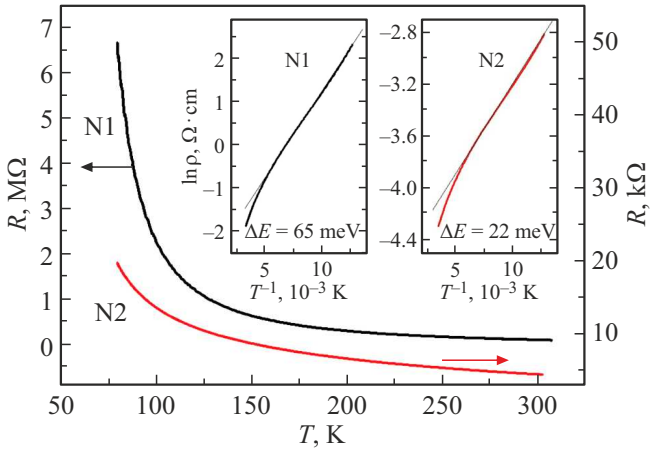

Figure 4. Temperature dependence of resistance for two samples. The left insert shows the definition of the activation energy for the film N1. The solid line shows the section $R(T)$ where activation dependence is observed. On the right insert the same dependencies for the film N2.

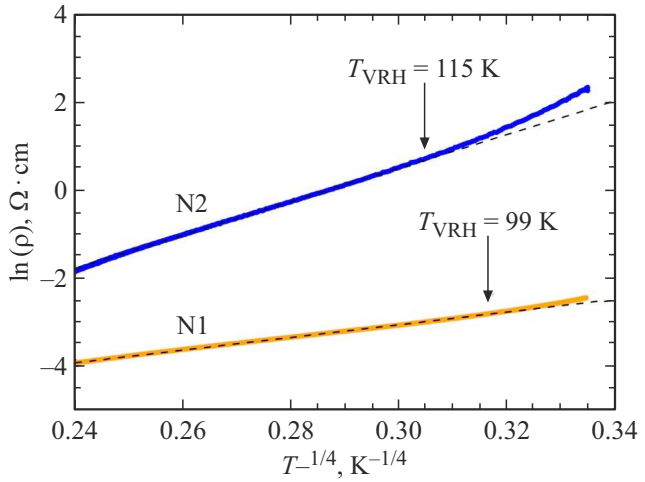

Figure 5. Dependence of the resistivity of ρ on $T^{-1/4}$ in the framework of the jump conduction model with variable jump length for epitaxial films Sr_2IrO_4.

during the transition from one sputtering mode to another leads to a change in the activation energy.

Another mechanism encountered in electronic transport in Sr_2IrO_4 thin films is hopping conductivity with Variable Hopping length (VRH) [16]. In the framework of this model, the temperature dependence is described by the ratio

$$\rho(T) = \rho_0 \exp\left[\left(\frac{T_0}{T}\right)^{1/4}\right] \quad (3)$$

where T_0 is a constant determined from the experiment. An approximation was performed by the function (3) of the dependence section up to the temperature T_{VRH}, below which the conductivity determined by the VRH mechanism is replaced by other electronic transport mechanisms (see Figure 5). According to the obtained parameters of the approximating curve, the values of the constant $T_0 = 2.0 \cdot 10^6$ K for the film N1 and $T_0 = 4.3 \cdot 10^4$ K for the film N2 were calculated. In the VRH model, the characteristic jump length l_{VRH} increases with decreasing temperature, like $T^{-1/4}$. In a thin film with a thickness of t, at a sufficiently low temperature, when l_{VRH} becomes larger than t, the three-dimensional hopping conductivity is replaced by other transport mechanisms. In work [16], the average jump length between the impurity centers along which charge carriers are transported is estimated through α — the radius of localization of the carriers at impurity centers

$$l_{VRH} = \frac{\alpha}{2}\left(\frac{T_0}{T}\right)^{1/4}. \quad (4)$$

VRH was observed at temperatures above the temperature of T_{VRH}, provided that the film thickness is $t \geq 2l_{VRH}$, which implies an estimate of the radius α by an order of magnitude

$$\alpha = t\left(\frac{T_{VRH}}{T_0}\right)^{1/4}. \quad (5)$$

For our samples, the T_{VRH} value was: for N1 $T_{VRH} \approx 115$ K, and for N2 $T_{VRH} \approx 99$ K. Calculated using the formula (4) The localization radii are equal: 1.3 nm for the sample without impurity N1 and 6.6 nm for the sample N2. Using the expression for the constant T_0 in terms of the radius of localization α and the density of localized states at the Fermi level $N(E_F)$: $T \approx (N(E_F) \cdot \alpha^3)^{-1}$ we obtained the following values $N(E_F) = 2.6 \cdot 10^{18}$ eV/cm^3 in the absence of an iridium impurity (sample N1) and $3.5 \cdot 10^{17}$ eV/cm^3 if present (sample N2). Despite such large differences in activation energy and the radius of localization of charge carriers, the crystal structure of the two samples is almost identical. Based on the available data, it can be assumed that the growth of iridium in the film occurs from iridium islands which appears at the beginning of the film grown. This can happen for several reasons, one of which is the different deposition rate, as well as the different angular dependencies of the deposition Sr and Ir [13].

From the analysis of the position of the X-ray peaks of the film (Figure 1), it follows that the presence of metallic iridium does not significantly change the crystal structure of the Sr_2IrO_4 film, but affects the electrical transport characteristics of the resulting film.

Thus, the analysis of the temperature dependence of the resistance of the epitaxial thin film Sr_2IrO_4 using various models in the appropriate temperature ranges allowed us to obtain a visual representation of the mechanisms of electronic transport at different temperatures. The revealed differences in the electron localization parameters indicate the influence of both the method and the sputtering modes on the transport properties of Sr_2IrO_4 films.

5. Conclusion

Using two technologies for the production of thin epitaxial films: DC cathode sputtering and pulsed current cathode sputtering, thin epitaxial films Sr_2IrO_4 were obtained. The dependences of resistivity on temperature obey the law of thermal activation at low (nitrogen) temperatures. At temperatures above 100 K, hopping conductivity was detected in these films. Based on these dependencies, the radii of localization of charge carriers from 1 to 7 nm are calculated. The pulsed mode of cathode sputtering allows for greater delocalization of charge carriers, which is important for the use of the material in spintronics, the strongest superconducting proximity effect should be observed in the film, which is required for the Josephson effect.

Funding

The research was carried out at the expense of a grant from the Russian Science Foundation (project No. 23-79-00010).

Conflict of interest

The authors state that they have no conflict of interest.

References

[1] H. Zhang, C. Liu, X. Qi, X. Dai, Z. Fang, S. Zhang. Nature Phys. **5**, 438 (2009).
[2] X. Wan, A.M. Turner, A. Vishwanath, S.Y. Savrasov. Phys. Rev. B **83**, 205101 (2011).
[3] Y.S. Hor, A.J. Williams, J.G. Checkelsky, P. Roushan, J. Seo, Q. Xu, H.W. Zandbergen, A. Yazdani, N.P. Ong, R.J. Cava. Phys. Rev. Lett. **104**, 057001 (2010).
[4] B.J. Kim, H. Jin, S.J. Moon, J.Y. Kim, B.G. Park, C.S. Leem, J. Yu, T.W. Noh, C. Kim, S.J. Oh, J.H. Park, V. Durairaj, G. Cao, E. Rotenberg. Phys. Rev. Lett. **101**, 076402 (2008).
[5] C. Cosio-Castaneda, G. Tavizon, A. Baeza, P. de la Mora, R. Escudero. J. Phys.: Condens. Mater **19**, 446210 (2007).
[6] J. Yang, L. Hao, P. Nanney, K. Noordhoek, D. Meyers, L. Horak, J. Sanchez, J.-H. Chu, C. Nelson, M.P.M. Dean, J. Liu. Appl. Phys. Lett. **114**, 182401 (2019).
[7] K. Nishio, H.Y. Hwang, Y. Hikita. APL Mater. **4**, 036102 (2016).
[8] Y.V. Kislinskii, K.Y. Constantinian, I.E. Moskal, N.V. Dubitskiy, A.M. Petrzhik, A.V. Shadrin, G.A. Ovsyannikov. Russ. Microelectron. **52**, S53 (2023).
[9] M. Petrzhik, K.Y. Constantinian, G.A. Ovsyannikov, A.V. Zaitsev, A.V. Shadrin, A.S. Grishin, Yu.V. Kislinski, G. Cristiani, G. Logvenov. Phys. Rev. **B 100**, 024501 (2019).
[10] G.A. Ovsyannikov, A.M. Petrzhik, I.V. Borisenko, A.A. Klimov, Yu.A. Ignatov, V.V. Demidov, S.A. Nikitov. J. Exp. Theor. Phys., **108**, 48 (2009).
[11] A.M. Petrzhik, G. Cristiani, G. Logvenov, A.E. Pestun, N.V. Andreev, Yu.V. Kislinskii, G.A. Ovsyannikov. Technical Physics Letters, **43**, *6*, 554 (2017).
[12] C. Lu, A. Quindeau, H. Deniz, D. Preziosi, D. Hesse, M. Alexe. Appl. Phys. Lett. **105**, 082407 (2014).
[13] V. Fuentes, L. Balcells, Z. Konstantinovic, B. Martínez, A. Pomar. Nanomaterials B **14**, *3*, 242 (2024).
[14] E.D. Specht, R.E. Clausing, L. Heathly. J. Mater. Res. **5**, 2351 (1990).
[15] H.C. Montgomery. J. Appl. Phys. **42**, 2971 (1971).
[16] Boris I. Shklovskii, Alex L. Efros. Electronic Properties of Doped Semiconductors. Springer Verlag, Berlin-Heidelberg (1984).

Translated by T.Zorina